

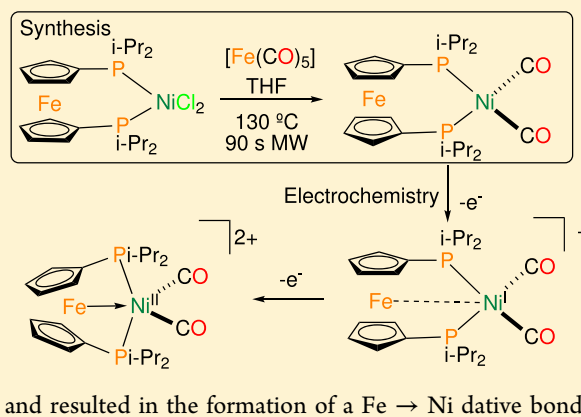
# Reductive Carbonylation of [NiCl<sub>2</sub>(dippf)] (dippf = 1,1'-Bis(diisopropylphosphino)ferrocene) with Fe(CO)<sub>5</sub> and (Spectro)electrochemistry of the Resulting [Ni(CO)<sub>2</sub>(dippf)]

Florian Döttinger and Mark R. Ringenberg\*<sup>✉</sup>

Institut für Anorganische Chemie, Universität Stuttgart, Pfaffenwaldring 55, 70550 Stuttgart, Germany

## Supporting Information

**ABSTRACT:** [NiCl<sub>2</sub>(dippf)] (**1**) (dippf = 1,1'-bis-(diisopropylphosphino)ferrocene) was synthesized from [NiCl<sub>2</sub>(dippf)] and [Fe(CO)<sub>5</sub>] at elevated temperature/pressure using microwave (MW) heating. **1** showed two oxidation waves in the cyclic voltammogram, and UV–vis–NIR spectroelectrochemistry (SEC) and IR SEC at –30 °C as well as computation support by means of DFT were used to determine the location and electron configuration after both oxidation events. The monocation [**1**]<sup>+</sup> showed a strong NIR absorption in the UV–vis–NIR spectrum that was a IVCT [Ni<sup>I</sup> → Fe<sup>II</sup>] and inverse IVCT (iIVCT) [Fe<sup>II</sup> → Ni<sup>I</sup>], and the IR SEC spectrum of [**1**]<sup>+</sup> showed multiple bands associated with two similar configurations, one where the spin is delocalized over both metal atoms and a second configuration where the spin is Ni localized. The second oxidation to [**1**]<sup>2+</sup> occurred at the Ni atom and resulted in the formation of a Fe → Ni dative bond.

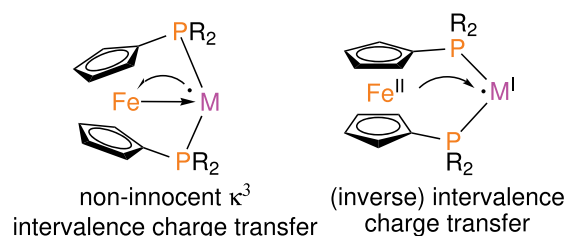


## INTRODUCTION

Many metalloenzymes contain hetero- and homo-bi(poly)-metallic clusters in their active sites, which in turn inspires bi(poly)metallic catalysts.<sup>1</sup> The burden of creating homo- and hetero-bimetallic complexes is facilitated by using ferrocene-based ligands with the form Fe(C<sub>5</sub>H<sub>4</sub>-D)<sub>2</sub>, where D = donor atom such as a P atom in 1,1'-bis(diisopropylphosphino)ferrocene (dippf).<sup>2–4</sup> A metallocene in the ligand backbone can enhance catalysis through cooperative affects and/or flexible binding modes. This property can be beneficial in advancing catalysis of “less common” oxidation states (Ni<sup>I/III</sup>) that are thought to play a role in some catalytic cycles.<sup>5–10</sup> Ferrocene-based ligands most often behave as a simple bis-chelate; however, many interesting exceptions have been reported,<sup>2,11–13</sup> including κ<sup>3</sup>-D<sub>2</sub>Fe<sub>2</sub>D-chelate where there is a Fe → TM (transition metal) interaction. This types of ligands can also behave noninnocently<sup>14</sup> by distributing electron spin/density from the central metal atom on the iron atom (Chart 1). The noninnocent behavior of these ligands is increased through the formation of a dative bond from the Fe → TM (Chart 1), and such interactions have been reported for carbonyl complexes of ruthenium, iron, manganese, and cobalt.<sup>11–13,15–18</sup> The iron atom in the ferrocene moiety can also provide electrons through a low-energy charge transfer, including inverse charge transfer (iIVCT), to an electron hole found on a transition metal center (Chart 1).<sup>11–13</sup>

Lang et al. reported that [Ni(CO)<sub>4</sub>] reacts with dppf (dppf = 1,1'-bis(diphenylphosphino)ferrocene) to form a mixture of [{Ni(CO)<sub>3</sub>]<sub>2</sub>(μ-dppf)] and [Ni(CO)<sub>2</sub>(dppf)], and the latter can be generated by heating the former to release [Ni(CO)<sub>4</sub>]

Chart 1. Noninnocent κ<sup>3</sup> and (Inverse) Intervalance Charge Transfer (iIVCT) of Ferrocene-Based Ligands

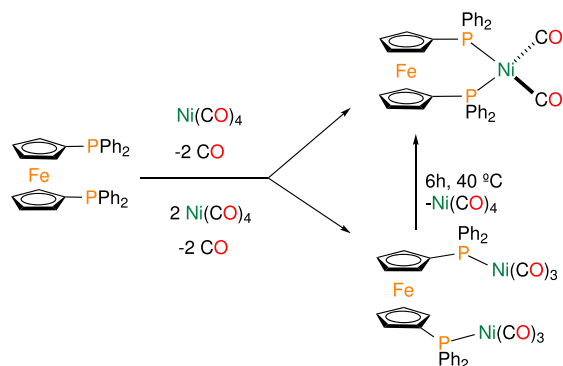
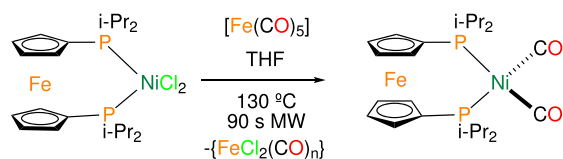


(Scheme 1).<sup>19</sup> Dicarboxynickel phosphine complexes can also be formed by reduction of [NiBr<sub>2</sub>(PR<sub>3</sub>)<sub>2</sub>] R = Ph, or Cy with Na-sand under a CO atmosphere; however, this method can result in additional side reactions to occur, such as P–C bond cleavage.<sup>20</sup> Most methods for forming L<sub>2</sub>Ni<sup>0</sup>(CO)<sub>2</sub> rely on the use of toxic, i.e., [Ni(CO)<sub>4</sub>], or harsh conditions that require specialized and cautious handling. Herein, we report the synthesis of [Ni(CO)<sub>2</sub>(dippf)] (**1**) in THF from [NiCl<sub>2</sub>(dippf)] with less hazardous [Fe(CO)<sub>5</sub>], which provides both the CO ligands and acts as the reductant (Scheme 2).

## RESULTS AND DISCUSSION

Synthesis of **1** was performed in a sealed tube microwave (MW) reactor where the reaction occurred rapidly (90 s) when a temperature of 130 °C was registered. The reaction

Received: December 6, 2018

Scheme 1.  $[\text{Ni}(\text{CO})_4]$  Reactions with Phosphine LigandsScheme 2. Synthesis of **[1]** Using  $[\text{Fe}(\text{CO})_5]$  as Reductant and CO Source

progress could be monitored by observing the change in color from green to yellow. The iron species were removed by filtration through a plug of neutral alumina, and after removal of the solvent the resulting yellow solid was **[1]**. **[1]** was crystallized from EtOH to yield X-ray quality crystals. The molecular structure of **[1]** is shown in Figure 1. Complex **[1]**

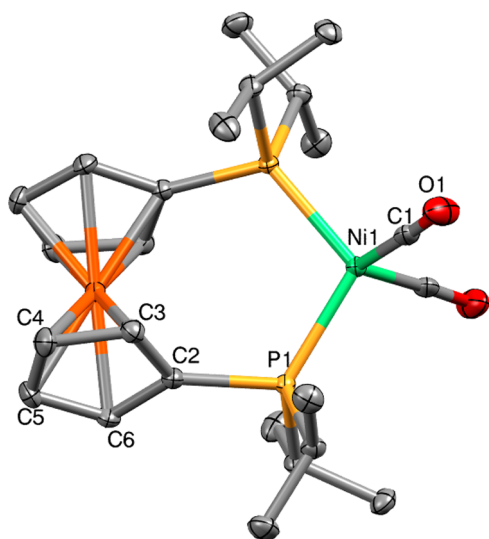


**Figure 1.** Molecular structure of **[1]** determined by X-ray diffraction. Ellipsoids shown at 50% probability. Hydrogen atoms were omitted for clarity.

crystallized in  $P12_1/C1$  (Table S1), the molecular structure (Figure 1) showed  $d_{\text{Fe-Ni}} = 4.243 \text{ \AA}$  with  $\text{P-Ni-P}$  of  $108.9^\circ$ , and the  $\eta^5\text{-C}_5\text{H}_4$ -ligands are staggered with a torsion angle  $\text{P1-C2-C2'-P1}' = 26.72^\circ$ . The molecular structure showed tetrahedral geometry at the Ni atom, and the  $\eta^5\text{-C}_5\text{H}_4$  ligands are not bent or distorted.

Starting from the molecule structure of **[1]**, a geometry-optimized model was generated using DFT calculations (see Supporting Information of coordinate tables). The frontier

Kohn–Sham orbitals for **[1]** are depicted in Figure 2. The HOMO resides over both metal ions but is dominated by an

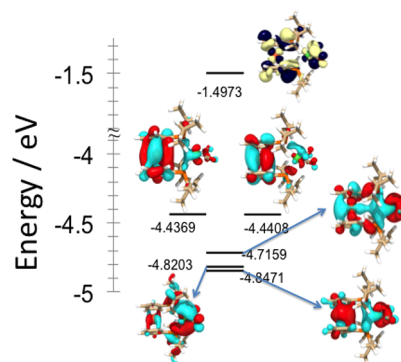


**Figure 2.** Energies of frontier orbitals from **[1]** determined by DFT calculations at TPSS/def2-TZVP/J level of theory.

orbital on the Fe atom. The HOMO–1 is nearly degenerate in energy to the HOMO, and it resides on the ferrocene moiety. The HOMO–2 is in phase MO located over both metal ions and the HOMO–4 is the out-of-phase MO, suggesting a degree of M–M communication. The  $d_{\text{Fe-Ni}} = 4.267 \text{ \AA}$  found in the molecular structure of **[1]** is outside the range for a Fe  $\rightarrow$  Ni bond; e.g.,  $([\text{Ni}(\text{Fe}(\text{C}_5\text{H}_4\text{S})_2)(\text{PMePh}_2)])$  was reported with a Fe–Ni distance  $2.886(1) \text{ \AA}^{21}$  and  $[\text{NiCl}(\text{ArF})(\text{dippf})]$  showed  $d_{\text{Fe-Ni}} = 3.498 \text{ \AA}$ , which is at the limits of a Fe–Ni interaction.<sup>22,23</sup> The HOMO–3 is located on the  $\text{Ni}(\text{CO})_2$  moiety. The LUMO for **[1]** is located at the ferrocene with some mixing from the dicarbonylnickel moiety. The UV–vis–NIR spectrum of **[1]** showed an absorption band at  $\lambda_{\text{max}}/\text{nm}$  [ $\epsilon/\text{M}^{-1} \text{ cm}^{-1}$ ] **[1]** =  $440$  [ $22727$ ] ( $251$ ). This band was described using TD-DFT (time dependence density functional theory) and was a combination of MLCT from the Ni and/or Fe to the Cp or CO ligands, see Figure S8 for a depiction of the orbital transitions.

The location and electron configuration of both oxidation events of **[1]** was further probed by (spectro)electrochemical methods. The cyclic voltammogram (CV) of **[1]** in  $0.1 \text{ M Bu}_4\text{NB}(\text{Ar}^F)_4/\text{CH}_2\text{Cl}_2$  ( $\text{B}(\text{Ar}^F)_4 = \text{Tetrakis}(3,5\text{-bis}(\text{trifluoromethyl})\text{phenyl})\text{borate}$ ) (Figure 3) showed a reversible oxidation event at  $E_{1/2}$  ( $[\text{1}]^{0/+}$ ) =  $-0.200 \text{ V}$  vs  $[\text{Fe}(\eta^5\text{-C}_5\text{H}_5)]$  ( $[\text{Fch}]^{0/+}$ ) (the internal standard for all potentials reported herein), and a second quasireversible oxidation at  $E_{1/2}$  ( $[\text{1}]^{+/2+}$ ) =  $0.340 \text{ V}$ . A comproportionation constant, i.e.,  $[\text{1}]^{12+}$

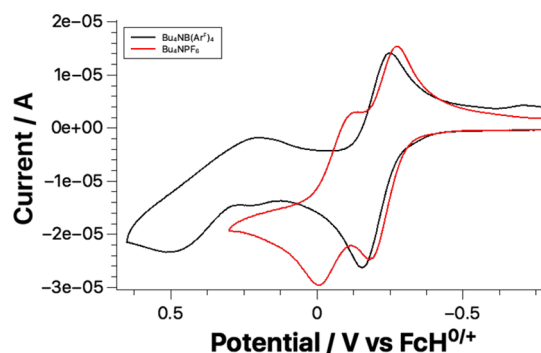


**Figure 3.** CV of  $1 \text{ mM}$  **[1]** in  $0.1 \text{ M Bu}_4\text{NPF}_6$  (red) or  $\text{Bu}_4\text{NB}(\text{Ar}^F)_4$  in  $\text{CH}_2\text{Cl}_2$  at  $50 \text{ mV s}^{-1}$ .

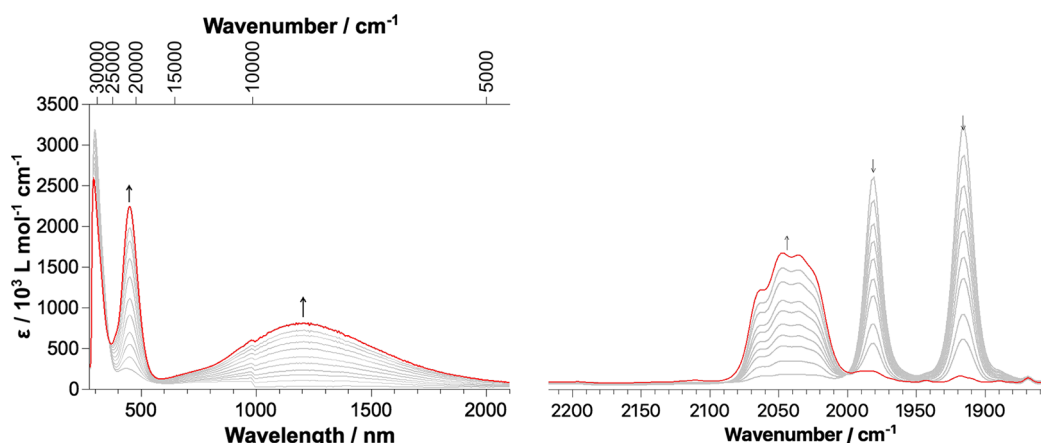


Figure 4. UV-vis-NIR and IR SEC spectra for  $[1]^{0/+}$  in 0.1 M  $\text{Bu}_4\text{NB}(\text{Ar}^{\text{F}})_4/\text{CH}_2\text{Cl}_2$  at  $-30\text{ }^\circ\text{C}$ .

Table 1. CT Bands from UV-Vis-NIR SEC of  $[1]$

complex	charge transfer	$\lambda_{\text{max}}$	$\nu_{\text{max}}$ (calc.)	$\nu_{1/2}$	$\epsilon_{\text{max}}$	$H_{\text{ab}}$
$[1]$	MLCT	420	22.779 (23.610)		0.255	
$[1]^+$	IVCT $\text{Fe}^{\text{II}} \rightarrow \text{Ni}^{\text{I}}$		7.607 (8.303)	1.654	0.520	430
	IVCT $\text{Ni}^{\text{I}} \rightarrow \text{Fe}^{\text{II}}$		9.665 (9.196)	2.038	0.420	483
$[1]^{2+}$	MMLCT	455	21.978 (22.070)		2.248	
	$\text{Fe}^{\text{II}} \rightarrow \text{Ni}^{\text{II}}$	575	17.393 (19.490)		1.568	
	$(\text{C}_5\text{H}_4)_2\text{Fe}^{\text{II}} \rightarrow \text{Ni}^{\text{II}}$	390	25.451 (24.386)		2.873	

$+ [1] \xrightleftharpoons{K_c} 2[1]^+$ ,  $K_c([1]) = 10^{\Delta E/59 \text{ mV}} = 10^{9.15}$ , was determined from the  $\Delta E$  and is consistent with a stable mixed-valence state for the monocation. Changing the electrolyte to  $\text{Bu}_4\text{NPF}_6$  caused the second redox wave to cathodically shift, and the  $\Delta E$  was smaller  $E_{1/2}([1]^{0/+}) = -0.200 \text{ V}$  and  $E_{1/2}([1]^{+/2+}) = 0.040 \text{ V}$ ,  $K_c([1]) = 10^{4.06}$  (Figure 3). The strong influence on  $K_c$  has been described in detail elsewhere<sup>24</sup> and is likely due to ion pairing with the monocation  $[1]^+$ .

The location of the oxidation, i.e., Ni or Fe based, is not evident based on the HOMO found during the DFT calculation; e.g.,  $[1]^+$  could have an electron configuration of  $[\text{Ni}^{\text{I}}\text{Fe}^{\text{II}}]$  or  $[\text{Ni}^{\text{0}}\text{Fe}^{\text{III}}]$  and  $[1]^{2+}$  could be either  $[\text{Ni}^{\text{I}}\text{Fe}^{\text{III}}]$  or  $[\text{Ni}^{\text{II}}\text{Fe}^{\text{II}}]$ . Further oxidations were not observed within the potential window provided by the solvent/electrolyte. In order to assign the electron configuration of the both metal atoms after oxidation, both redox events were studied by means of UV-vis-NIR/IR spectroelectrochemistry (SEC); however, both SEC experiments were performed at low temperature ( $-30\text{ }^\circ\text{C}$ ) due to nonisobestic behavior at room temperature. Additionally, attempts to chemically oxidize  $[1]$  with  $[\text{FCH}]\text{-B}(\text{Ar}^{\text{F}})_4$  at  $-30$  in  $\text{Et}_2\text{O}$ , THF, or  $\text{CH}_2\text{Cl}_2$  resulted in loss of the CO signals.

The oxidation event  $[1]^{0/+}$  was monitored by UV-vis-NIR SEC at  $-30\text{ }^\circ\text{C}$  in 0.1  $\text{Bu}_4\text{NB}(\text{Ar}^{\text{F}})_4/\text{CH}_2\text{Cl}_2$  due to the large separation of the two oxidation events. Oxidation resulted in the band at  $\lambda_{\text{max}}/\text{nm}$  [ $\text{cm}^{-1}$ ]  $[1] = 439$  [22 779] to be replaced by new bands at  $\lambda_{\text{max}}/\text{nm}$  [ $\text{cm}^{-1}$ ] ( $\epsilon/\text{M}^{-1} \text{cm}^{-1}$ )  $[1]^+ = 468$  [21 367] (1596), 709 [13 175] (162) 1276 [7836] (640) (Figure 4 and Table 1), see Figure S4 for spectrum fitting. The large NIR band was also observed for other metal-carbonyls containing ferrocene-based ligands,<sup>11–13</sup> although the NIR band for  $[1]^+$  was more intense and broader than those previously described.

The infrared SEC spectrum at  $-30\text{ }^\circ\text{C}$  in 0.1  $\text{Bu}_4\text{NB}(\text{Ar}^{\text{F}})_4/\text{CH}_2\text{Cl}_2$  of  $[1]^{0/+}$  showed the two bands for  $\nu_{\text{CO}}[1] = 1983$ ,

1915  $\text{cm}^{-1}$  shifted to higher energy bands at and  $\nu_{\text{CO}}[1]^+ = 2064$ , 2046, 2035, 2023  $\text{cm}^{-1}$  (Figure 4). The role of the electrolyte is clearly seen when the IR SEC was performed in 0.1  $\text{Bu}_4\text{NPF}_6/\text{CH}_2\text{Cl}_2$  (Figures S6 and S7) where mixtures of all three redox states were observed in the spectra, although a similar spectral response was also observed. The  $\Delta\nu_{\text{CO}}[1] = 80/106 \text{ cm}^{-1}$  for  $[1]^{0/+}$  is larger than expected if the oxidation occurred at the ferrocene moiety.<sup>25–27</sup> The first oxidation event was assigned to  $\text{Ni}^{0/1}$  oxidation on the basis of the IR SEC spectrum; however, four CO bands from  $\nu_{\text{CO}}[1]^+$  are too numerous for a single dicarbonylnickel product.

Open shell calculations on  $[1]^+$  revealed a distorted trigonal bipyramidal molecular geometry with a  $d_{\text{Fe-Ni}}[1]^+ = 3.873 \text{ \AA}$ , and the spin density was distributed nearly equally over both Fe and Ni sites (Mulliken spin Ni: 0.43, Fe: 0.39). A DFT potential energy surface scan was performed in which the  $d_{\text{Fe-Ni}}$  was scanned from 2.6–5  $\text{Å}$ . The energy surface is shown in Figure 5 and shows the lowest energy configuration with  $d_{\text{Fe-Ni}}[1]^+ = 3.873 \text{ \AA}$ , and second configuration was found at +4 kcal  $\text{mol}^{-1}$  above the global minimum energy with  $d_{\text{Fe-Ni}}[1]^+ = 4.511 \text{ \AA}$ , and the spin was not as evenly

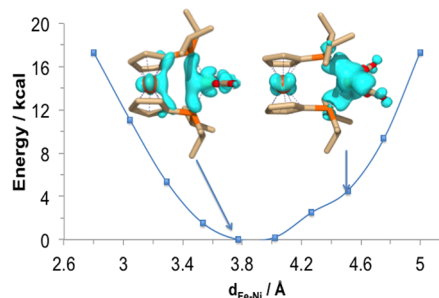
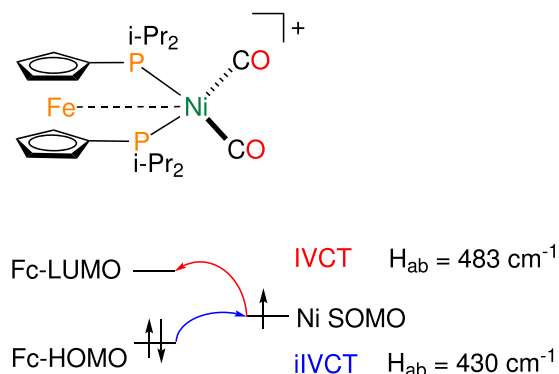


Figure 5. Potential energy surface scan for  $[1]^+$  along Fe-Ni axis with spin density shown in light blue.

distributed, locating more at the Ni site (Mulliken spin Ni: 0.46, Fe: 0.22) (Figure 5). The appearance of multiple bands in the IR SEC spectrum of  $[1]^+$  is conjectured to be a result of the weak Fe–Ni interaction, which allows for two close energy configurations to be observed, one where the electron spin is distributed almost equally over both metal atoms that results in a smaller  $\Delta\nu_{\text{CO}}[1]^+ = 80 \text{ cm}^{-1}$ ,<sup>11,12</sup> and one where the spin density is primarily located at the Ni atom  $\Delta\nu_{\text{CO}}[1]^+ = 106 \text{ cm}^{-1}$ .<sup>25–27</sup>

The UV–vis–NIR spectrum of the lower energy geometry of open-shell  $[1]^+$  was described using TD-DFT calculations. The near IR transition at  $7836 \text{ cm}^{-1}$  was described as a combination of two different intervalence charge transfer (IVCT) bands, one at  $7607 \text{ cm}^{-1}$  and another at  $9665 \text{ cm}^{-1}$  (Figure S4). The higher energy band at  $9665 \text{ cm}^{-1}$  was a classic IVCT from a low to high valent metal ion ( $\text{Ni}^{\text{I}} \rightarrow \text{Fe}^{\text{II}}$ ), while the lower energy band at  $7607 \text{ cm}^{-1}$  was an inverse intervalence charge transfer (iIVCT), i.e., from a high to low valent metal ion ( $\text{Fe}^{\text{II}} \rightarrow \text{Ni}^{\text{I}}$ ) (Scheme 3). TD-DFT

### Scheme 3. $\text{Ni}^{\text{I}} \rightarrow \text{Fe}^{\text{II}}$ iIVCT and $\text{Fe}^{\text{II}} \rightarrow \text{Ni}^{\text{I}}$ IVCT Exchange Energy ( $H_{\text{ab}}$ ) Determined from Analysis of NIR Band



calculations were also performed on the higher energy geometry of  $[1]^+$ , and showed similar iIVCT ( $6610 \text{ cm}^{-1}$ ) and IVCT ( $13507 \text{ cm}^{-1}$ ), see Figure S10 for depiction of transitions. These data on both geometries showed similar transitions in the UV–vis–NIR spectrum; however, the lower energy geometry fits closer the spectrum in Figure 4, as the higher energy IVCT band at  $13507 \text{ cm}^{-1}$  was not observed.

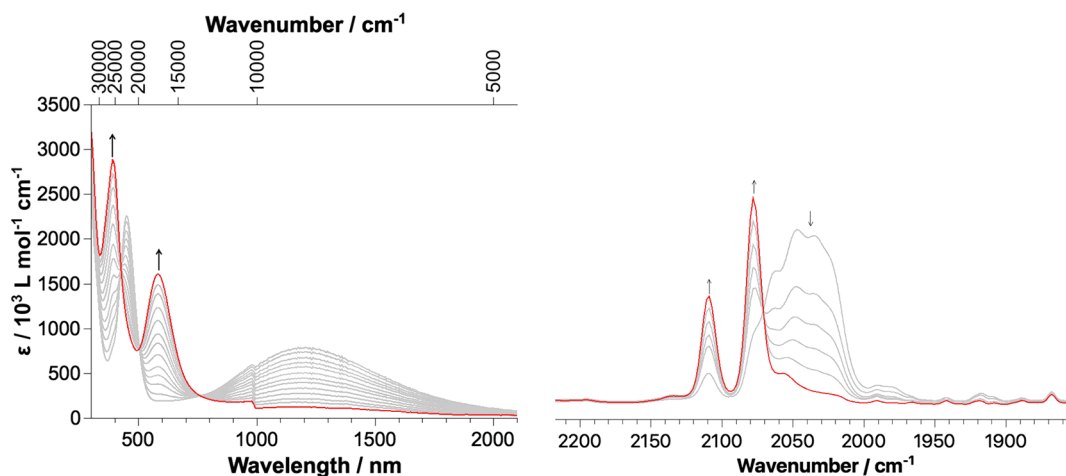


Figure 6. UV–vis–NIR and IR SEC spectra for  $[1]^{+/2+}$  in 0.1 M  $\text{Bu}_4\text{NB}(\text{Ar}^{\text{F}})_4/\text{CH}_2\text{Cl}_2$  at  $-30 \text{ }^\circ\text{C}$ .

The iIVCT is possible because of the different ligation, i.e.,  $\eta^5\text{-C}_5\text{H}_4$  donating for iron and  $\pi$ -accepting CO for the Ni. Performing a Hush analysis on these two bands show  $H_{\text{ab}} = 430 \text{ cm}^{-1}$  (iIVCT) and  $H_{\text{ab}} = 483 \text{ cm}^{-1}$  (IVCT), where  $d_{\text{Fe-Ni}} = 4.227 \text{ \AA}$  (calc), are consistent with a valence localized system.<sup>28–30</sup>

The UV–vis–NIR SEC spectrum at  $-30 \text{ }^\circ\text{C}$  (Figure 6) in 0.1  $\text{Bu}_4\text{NB}(\text{Ar}^{\text{F}})_4/\text{CH}_2\text{Cl}_2$  for  $[1]^{+/2+}$  caused a decrease in NIR band and two new absorption bands to appear at  $\lambda_{\text{max}}/\text{nm}$  [ $\text{cm}^{-1}$ ] ( $\epsilon/\text{M}^{-1} \text{ cm}^{-1}$ )  $[1]^{2+} = 575$  [17393] (1568) and 390 [25451] (2873) (Figure 6 and Table 1). The band at 575 nm is typical for a  $\text{Fe} \rightarrow \text{TM}$  interaction.<sup>23,31</sup> These two bands were described using TD-DFT and the lower energy band was a MMCT and the higher energy band was an ICVT from  $\text{Fe} \rightarrow \text{Ni}$ , see Figure S11 for a depiction of the transitions. The IR SEC spectrum at  $-30 \text{ }^\circ\text{C}$  for  $[1]^{+/2+}$  (Figure 6) showed the bands from  $[1]^+$  converged into two bands  $\nu_{\text{CO}}[1]^{2+} = 2108$ , and  $2077 \text{ cm}^{-1}$  (Figure 6). The two bands were consistent with a trigonal-bipyramidal configuration with the two CO-bands equatorially coordinated.<sup>32–34</sup>

The closed-shell DFT calculations for the dication  $[1]^{2+}$  showed a short  $d_{\text{Fe-Ni}}[1]^{2+} = 2.973$  (calc.)  $\text{\AA}$ , and the intrinsic bonding orbital (IBO)<sup>35</sup> shows the dative bond from the Fe to the Ni atom (Figure 7). A DFT potential energy surface scan

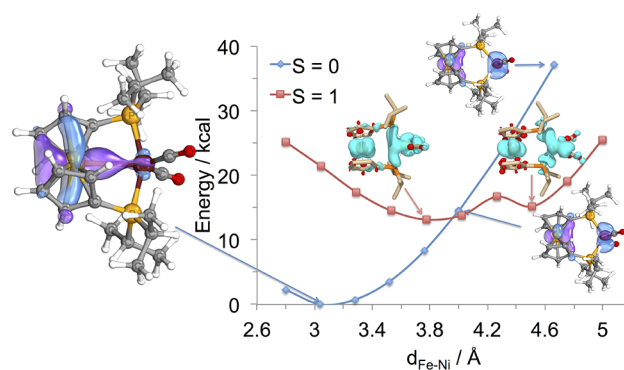


Figure 7. Intrinsic bond orbital (IBO)<sup>35</sup> generated from closed shell calculations of  $[1]^{2+}$  showing  $\text{Fe} \rightarrow \text{Ni}$  bonding orbital. Potential energy surface scan for  $[1]^{2+}$  along  $\text{Fe-Ni}$  axis  $S = 0$  (blue)  $S = 1$  (red).

was performed in which the  $d_{\text{Fe-Ni}}$  was scanned from 2.6–5 Å. Scanning along the Fe–Ni axis showed the energy minimum at  $d_{\text{Fe-Ni}} = 2.973$  Å, increasing the distance caused an increase in the energy. Elongation of the Fe–Ni distance did not afford a reasonable minimum structure with a singlet ground state. A proposed intersystem crossing to a triplet state was observed at 4 Å. A PES scan of the triplet state showed two energy minima that were both higher in energy than the singlet state. These minima were found at  $d_{\text{Fe-Ni}} = 3.8$  and 4.6 Å, which corresponded to a delocalized triplet state with spin density over both Fe and Ni atoms ( $d_{\text{Fe-Ni}} = 3.8$ , Mulliken spin Ni: 0.71, Fe: 1.18) and ( $d_{\text{Fe-Ni}} = 4.6$ , Mulliken spin Ni: 0.58, Fe: 1.24) (Figure 7). The result of this intersystem crossing is that the Fe–Ni bond energy is about 15 kcal mol<sup>-1</sup>, which falls at the lower energy range for “typical” Fe–TM bonds that have a range of 22–24 kcal mol<sup>-1</sup>.<sup>23</sup> This behavior was also observed in a nickel complex containing a ferrocene-based ligand, e.g.,  $[\{\text{Fe}(\text{C}_5\text{H}_4\text{NIm})_2\}\text{Ni}(\text{NCMe})_2]^{2+}$  Im = imidazole,<sup>36</sup> which had a BDE(Fe–Ni) = 11.3 kcal mol<sup>-1</sup>.

## CONCLUSIONS

The complex  $[\text{Ni}(\text{CO})_2(\text{dippf})]$  [1] was synthesized by reduction of  $[\text{NiCl}_2(\text{dippf})]$  and transfer of CO ligands from less toxic and readily available  $[\text{Fe}(\text{CO})_5]$  at elevated temperature under MW heating. DFT calculations on [1] showed the HOMO to be delocalized over both metal atoms, which complicated the assignment of the two oxidation events observed in the CV. UV–vis–NIR SEC spectrum of  $[\text{1}]^+$  showed a large NIR absorption, which was described according to TD-DFT as a IVCT  $[\text{Ni}^{\text{I}} \rightarrow \text{Fe}^{\text{II}}]$  and inverse IVCT (iIVCT)  $[\text{Fe}^{\text{II}} \rightarrow \text{Ni}^{\text{I}}]$  or hole transfer. The IR SEC spectrum of  $[\text{1}]^+$  shows four bands, which was ascribed to two similar configurations, one which contains a Fe → Ni dative bond where the spin is delocalized over both metal atoms, and a second configuration where the spin is primarily Ni localized; therefore,  $[\text{Fe}^{\text{II}}\text{Ni}^{\text{I}}]$  was assigned as the electron configuration of  $[\text{1}]^+$ . The second oxidation to  $[\text{1}]^{2+}$  results in the formation of a Fe → Ni dative bond, which was found during DFT calculations and was further supported by UV–vis–NIR/IR SEC. Attempts to calculate the BDE(Fe–Ni) of  $[\text{1}]^{2+}$  were complicated by an intersystem crossing from a singlet state to a triplet state, resulting in BDE(Fe–Ni) = 15 kcal mol<sup>-1</sup>. The ferrocene-based phosphine ligands can be used to help support the higher oxidation states ( $\text{Ni}^{\text{I}}$  and  $\text{Ni}^{\text{II}}$ ) of metal atoms through the formation of a Fe interaction and by providing electrons through low energy charge transfer from the Fe to the Ni atom.

## EXPERIMENTAL SECTION

Microwave (MW) reactions were carried out in a 30 mL glass tube with a maximum volume of 10 mL in Monowave 400 microwave synthesis reactor by Anton Paar. <sup>1</sup>H and <sup>31</sup>P{<sup>1</sup>H} NMR spectra were obtained on a Bruker AC 250 spectrometer. <sup>1</sup>H NMR spectra were referenced versus residual solvent peak and <sup>31</sup>P{<sup>1</sup>H} NMR spectra were referenced against an external standard H<sub>3</sub>PO<sub>4</sub>. IR spectra were obtained using a Nicolet 6700 FT-IR instrument. UV–vis–NIR absorption spectra were recorded on J&M TIDAS spectrophotometer. Cyclic voltammetry was carried out in 0.1 M Bu<sub>4</sub>NB(Ar<sup>F</sup>)<sub>4</sub>/CH<sub>2</sub>Cl<sub>2</sub> solutions using a three-electrode configuration (glassy carbon working, Pt wire counter electrodes, and Ag reference) and were performed using a Metrohm Autolab potentiostat. The ferrocene/ferrocenium ( $[\text{FcH}]^{0/+}$ ) couple served as internal reference to all potentials reported herein. Tetrabutylammonium tetrakis[3,5-bis-(trifluoromethyl)phenyl]borate synthesis can be found in the

Supporting Information. Spectroelectrochemistry was performed using an optically transparent thin-layered electrode (OTTLE) cooled using a liquid nitrogen cryostat previously described.<sup>37</sup> X-ray diffraction data were collected using a Bruker Kappa Apex2duo diffractometer. The structures were solved using Patterson method and refined by full-matrix least-squares techniques on F2 using the OLEX2 program.<sup>38</sup> The absorption corrections were done by multiscan technique. All non-hydrogen atoms were anisotropically refined. Hydrogen atoms were included in the refinement process as per the riding model.

Density functional theory (DFT) calculations were performed using the solid-state structures of [1], and the closed-shell structure of  $[\text{1}]^{2+}$  was determined by removing 2e<sup>-</sup> from the structure of [1]. A computational analysis was performed by means of restricted Kohn–Sham density functional theory (DFT) using TPSS<sup>39</sup> functional in combination with the D3 dispersion correction<sup>40</sup> with the def2-TZVP<sup>41,42</sup> and Weigend J auxiliary basis set.<sup>41,42</sup> Geometry optimizations were realized with the ORCA program package with TightSCF convergence ( $1.0 \times 10^{-7}$  au).<sup>43</sup> Solvation in CH<sub>2</sub>Cl<sub>2</sub> was modeled using the CPCM solvation model.<sup>44</sup> Open-shell calculations on the structure  $[\text{1}]^+$  and  $[\text{1}]^{2+}$  were determined by subtracting 1e<sup>-</sup> or 2e<sup>-</sup>, respectively, and calculations were performed by means of unrestricted Kohn–Sham DFT using the same basis set, functionals, and solvent models as the closed-shell structures.

1,1'-Bis(diisopropylphosphino)ferrocene was purchased from ABCR and used without further purification. THF was distilled from sodium-benzophenone and stored over 3 Å molecular sieves. NaB(Ar<sup>F</sup>)<sub>4</sub> was synthesized according to literature procedure.<sup>45</sup>

1,1'-Bis(diisopropylphosphino)ferrocenedichloride was made according to modified reported procedure<sup>46</sup> by heating an equal molar  $[\text{Ni}(\text{H}_2\text{O})_6]\text{Cl}_2$  (568 mg, 2.39 mmol) and dippf (999 mg, 2.39 mmol) solution in 2-propanol:methanol 2:1 (75 mL), and cooling the solution to –30 °C yielded green microcrystals that were collected by filtration and dried at reduced pressure. Yield 79%. The substance was used in the next step without further purification.

**1,1'-Bis(diisopropylphosphino)ferrocenedicarbonylnickel [1].** A 30 mL MW reaction tube was charged with  $[\text{NiCl}_2(\text{dippf})]$  (480 mg, 0.70 mmol),  $[\text{Fe}(\text{CO})_5]$  (411 mg, 2.10 mmol) and THF (10 mL). The reaction solution was purged with N<sub>2</sub> for 5 min. The reaction tube was placed in the MW, and it was heated to 130 °C for 3 min until the color turned from green to yellow (90 s). The resulting reaction solution was cooled to room temperature, and the solution was passed quickly through as small plug of neutral alumina. The THF was removed at reduced pressure, and the resulting sticky yellow solid was crystallized from hot ethanol, yield = 75%. <sup>1</sup>H NMR (CD<sub>2</sub>Cl<sub>2</sub>) δ 5.32 (s, CH<sub>2</sub>Cl<sub>2</sub>), 4.27 (4H, s), 4.23 (4H, s), 2.14 (4H, m), 1.25–1.70 (24H, m). <sup>31</sup>P{<sup>1</sup>H} NMR (CD<sub>2</sub>Cl<sub>2</sub>) δ 41.38 (s) ppm. CH: elemental analysis calcd. (%) for C<sub>24</sub>H<sub>36</sub>FeNiO<sub>2</sub>P<sub>2</sub>(CH<sub>2</sub>Cl<sub>2</sub>)<sub>0.25</sub>: C 52.55, H, 6.64. Found: C 52.77, H 6.62.

## ASSOCIATED CONTENT

### Supporting Information

The Supporting Information is available free of charge on the ACS Publications website at DOI: 10.1021/acs.organomet.8b00881.

Fitted UV–vis–NIR and IR spectrum of  $[\text{1}]^+$ , TD-DFT, EDDM, crystallographic tables, and coordinates determined by DFT (PDF)

XYZ files (ZIP)

### Accession Codes

CCDC 1874489 contains the supplementary crystallographic data for this paper. These data can be obtained free of charge via [www.ccdc.cam.ac.uk/data\\_request/cif](http://www.ccdc.cam.ac.uk/data_request/cif), or by emailing [data\\_request@ccdc.cam.ac.uk](mailto:data_request@ccdc.cam.ac.uk), or by contacting The Cambridge Crystallographic Data Centre, 12 Union Road, Cambridge CB2 1EZ, UK; fax: +44 1223 336033.

## AUTHOR INFORMATION

## Corresponding Author

\*E-mail: [mark.ringenberg@iac.uni-stuttgart.de](mailto:mark.ringenberg@iac.uni-stuttgart.de). Phone: +49 (0)711 685-64196. Fax: +49 (0)711 685-64165.

## ORCID

Mark R. Ringenberg: 0000-0001-7585-5757

## Notes

The authors declare no competing financial interest.

## ACKNOWLEDGMENTS

The authors thank Prof. Wolfgang Kaim for support and continued advice. Dr. Wolfgang Frey is thanked for advice and crystallographic measurements. M.R.R. gratefully acknowledges support by the state of Baden-Württemberg through bwHPC and the German Research Foundation (DFG) through grant no. INST 40/467-1 FUGG for access to the Justus cluster. Funding provided by Institut für Anorganische Chemie, Universität Stuttgart, Stuttgart DE.

## REFERENCES

- (1) Peters, R. *Cooperative Catalysis*; Wiley-VCH: Weinheim, 2015.
- (2) Stepnicka, P. *Ferrocenes: Ligands, Materials and Biomolecules*; John Wiley & Sons, Inc., 2008.
- (3) Togni, A. *Metallocenes*; Wiley-VCH Verlag GmbH, 2008; pp 685–721.
- (4) Astruc, D. Why is Ferrocene so Exceptional? *Eur. J. Inorg. Chem.* **2017**, 2017, 6–29.
- (5) Lin, C.-Y.; Power, P. P. Complexes of Ni(i): a "rare" oxidation state of growing importance. *Chem. Soc. Rev.* **2017**, 46, 5347–5399.
- (6) Bajo, S.; Laidlaw, G.; Kennedy, A. R.; Sproules, S.; Nelson, D. J. Oxidative Addition of Aryl Electrophiles to a Prototypical Nickel(0) Complex: Mechanism and Structure/Reactivity Relationships. *Organometallics* **2017**, 36, 1662–1672.
- (7) Saraev, V. V.; Kraikivskii, P. B.; Vilms, A. I.; Zelinskii, S. N.; Yunda, A. Y.; Danilovtseva, E. N.; Kuzakov, A. S. Cyclotrimerization and linear oligomerization of phenylacetylene on the nickel(I) monocyclopentadienyl complex CpNi(PPh<sub>3</sub>)<sub>2</sub>. *Kinet. Catal.* **2007**, 48, 778–784.
- (8) Eckert, N. A.; Dinescu, A.; Cundari, T. R.; Holland, P. L. A T-Shaped Three-Coordinate Nickel(I) Carbonyl Complex and the Geometric Preferences of Three-Coordinate d9 Complexes. *Inorg. Chem.* **2005**, 44, 7702–7704.
- (9) Schwab, M. M.; Himmel, D.; Kacprzak, S.; Kratzert, D.; Radtke, V.; Weis, P.; Ray, K.; Scheidt, E.-W.; Scherer, W.; de Bruin, B.; Weber, S.; Krossing, I. [Ni(cod)<sub>2</sub>][Al(ORF)<sub>4</sub>], a Source for Naked Nickel(I) Chemistry. *Angew. Chem., Int. Ed.* **2015**, 54, 14706–14709.
- (10) Sondermann, C.; Ringenberg, M. R. Tuning the overpotential of electrocatalytically active cyclopentadienylnickel complexes containing 1,4-diaza-1,3-butadienes (DAB) for proton reduction. *Dalton Trans* **2017**, 46, 5143–5146.
- (11) Ringenberg, M. R.; Schwilk, M.; Wittkamp, F.; Apfel, U.-P.; Kaim, W. Organometallic Fe-Fe Interactions: Beyond Common Metal-Metal Bonds and Inverse Mixed-Valent Charge Transfer. *Chem. - Eur. J.* **2017**, 23, 1770–1774.
- (12) Ringenberg, M. R.; Wittkamp, F.; Apfel, U.-P.; Kaim, W. Redox Induced Configurational Isomerization of Bisphosphine-Tricarbonyliron(I) Complexes and the Difference a Ferrocene Makes. *Inorg. Chem.* **2017**, 56, 7501–7511.
- (13) Schäfer, K. M.; Reinders, L.; Fiedler, J.; Ringenberg, M. R. Twisting and Tilting 1,1'-Bis(dialkylphosphino)ferrocene with Low Valent Tricarbonylmanganese(I to -I). *Inorg. Chem.* **2017**, 56, 14688–14696.
- (14) Kaim, W.; Schwederski, B. Non-innocent ligands in bioinorganic chemistry - An overview. *Coord. Chem. Rev.* **2010**, 254, 1580–1588.
- (15) Kluwer, A. M.; Krafft, M. J.; Hartenbach, I.; de Bruin, B.; Kaim, W. Hydroformylation of 1-Octene Mediated by the Cobalt Complex [CoH(dchpf)(CO)<sub>2</sub>]. *Top. Catal.* **2016**, 59, 1787–1792.
- (16) Krafft, M. J.; Bubrin, M.; Paretzki, A.; Lissner, F.; Fiedler, J.; Zálaiš, S.; Kaim, W. Identifying Intermediates of Sequential Electron and Hydrogen Loss from a Dicarboxylcobalt Hydride Complex. *Angew. Chem., Int. Ed.* **2013**, 52, 6781–6784.
- (17) Krafft, M. J.; Lissner, F.; Fiedler, J.; Kaim, W. Cobalt Carbonyl Hydrides with 1,1'-Diphosphinylferrocene Ligands - Structural and Electrochemical Diversity. *Z. Anorg. Allg. Chem.* **2017**, 643, 1971–1977.
- (18) Sixt, T.; Sieger, M.; Krafft, M. J.; Bubrin, D.; Fiedler, J.; Kaim, W. Ambi-Valence Taken Literally: Ruthenium vs Iron Oxidation in (1,1'-Diphosphinoferrocene)ruthenium(II) Hydride and Chloride Complexes as Deduced from Spectroelectrochemistry of the Heterodimetallic "Mixed-Valent" Intermediates. *Organometallics* **2010**, 29, 5511–5516.
- (19) Schaarschmidt, D.; Kühnert, J.; Tripke, S.; Alt, H. G.; Görl, C.; Ruffer, T.; Ecorchard, P.; Walfort, B.; Lang, H. Ferrocenyl phosphane nickel carbonyls: Synthesis, solid state structure, and their use as catalysts in the oligomerization of ethylene. *J. Organomet. Chem.* **2010**, 695, 1541–1549.
- (20) Nobile, C. F.; Vasapollo, G.; Giannoccaro, P.; Sacco, A. Dicyclohexylphosphido complexes of nickel(I). *Inorg. Chim. Acta* **1981**, 48, 261–263.
- (21) Takemoto, S.; Kuwata, S.; Nishibayashi, Y.; Hidai, M. Synthesis of Heterobimetallic Fe-M (M = Ni, Pd, Pt) Complexes Containing the 1,1'-Ferrocenedithiolato Ligand and Their Conversion to Trinuclear Complexes. *Inorg. Chem.* **1998**, 37, 6428–6434.
- (22) Jover, J.; Miloserdov, F. M.; Benet-Buchholz, J.; Grushin, V. V.; Maseras, F. On the Feasibility of Nickel-Catalyzed Trifluoromethylation of Aryl Halides. *Organometallics* **2014**, 33, 6531–6543.
- (23) Ringenberg, M. Beyond Common Metal-Metal Bonds,  $\kappa^3$ Bis(donor)ferrocenyl→Transition Metal Interaction. *Chem. - Eur. J.* **2018**, DOI: 10.1002/chem.201803150.
- (24) D'Alessandro, D. M.; Keene, F. R. A cautionary warning on the use of electrochemical measurements to calculate comproportionation constants for mixed-valence compounds. *Dalton Trans* **2004**, 3950–3954.
- (25) Hartl, F.; Vlcek, A.; DeLearie, L. A.; Pierpont, C. G. Oxidative substitution of pentacarbonylmanganese(1-) by 3,5-di-tert-butyl-1,2-benzoquinone. Synthesis and characterization of the unsaturated Mn(CO)<sub>3</sub>(DBCat)<sup>-</sup> anion. *Inorg. Chem.* **1990**, 29, 1073–1078.
- (26) Sherlock, S. J.; Boyd, D. C.; Moasser, B.; Gladfelter, W. L. Homogeneous catalytic carbonylation of nitroaromatics. 4. Preparation and characterization of ruthenium radical cations. *Inorg. Chem.* **1991**, 30, 3626–3632.
- (27) Therien, M. J.; Troglor, W. C. Tricarbonylbis(phosphine)iron(I) cation radicals. A spectroscopic and theoretical study. *J. Am. Chem. Soc.* **1986**, 108, 3697–3702.
- (28) Klenk, S.; Rupf, S.; Suntrup, L.; van der Meer, M.; Sarkar, B. The Power of Ferrocene, Mesoionic Carbenes, and Gold: Redox-Switchable Catalysis. *Organometallics* **2017**, 36, 2026–2035.
- (29) Packheiser, R.; Jakob, A.; Ecorchard, P.; Walfort, B.; Lang, H. Diphenylphosphinoferrocene Gold(I) Acetylides: Synthesis of Hetero- and Heterotetrametallic Transition Metal Complexes. *Organometallics* **2008**, 27, 1214–1226.
- (30) Rößler, K.; Ruffer, T.; Walfort, B.; Packheiser, R.; Holze, R.; Zharnikov, M.; Lang, H. Synthesis, characterization and electrochemical behavior of unsymmetric transition metal-terminated biphenyl ethynyl thiols. *J. Organomet. Chem.* **2007**, 692, 1530–1545.
- (31) Sato, M.; Shigeta, H.; Sekino, M.; Akabori, S. Synthesis, some reactions, and molecular structure of the Pd(BF<sub>4</sub>)<sub>2</sub> complex of 1,1'-bis(diphenylphosphino)ferrocene. *J. Organomet. Chem.* **1993**, 458, 199–204.
- (32) Jones, R. A.; Stuart, A. L.; Atwood, J. L.; Hunter, W. E. Substitution reactions of di-tert-butylphosphido complexes of nickel(I). Crystal structures of Ni<sub>2</sub>[μ-(Me<sub>3</sub>C)2P]2(CO)2(PMe<sub>3</sub>) (Ni-

- Ni) and Ni<sub>2</sub>[μ-(Me<sub>3</sub>C)<sub>2</sub>P]<sub>2</sub>(CO)<sub>3</sub> (Ni-Ni). *Organometallics* **1983**, *2*, 874–878.
- (33) Ritchey, J. M.; Zozulin, A. J.; Wroblewski, D. A.; Ryan, R. R.; Wasserman, H. J.; Moody, D. C.; Paine, R. T. An organothorium-nickel phosphido complex with a short thorium-nickel distance. The structure of Th( $\eta^5$ -C<sub>5</sub>Me<sub>5</sub>)<sub>2</sub>(μ-PPh<sub>2</sub>)<sub>2</sub>Ni(CO)<sub>2</sub>. *J. Am. Chem. Soc.* **1985**, *107*, 501–503.
- (34) Fischer, K.; Vahrenkamp, H. Stereochemie der Metall-Metall-Bindung Die Strukturen der Verbindungen (CO)<sub>4</sub>Cr[μ-PMe<sub>2</sub>]<sub>2</sub>Ni(CO)<sub>2</sub> und (CO)<sub>3</sub>Fe[μ-PMe<sub>2</sub>,μ-I]Fe(CO)<sub>3</sub> mit je zwei verschiedenen Komplexhälften. *Z. Anorg. Allg. Chem.* **1981**, *475*, 109–115.
- (35) Knizia, G. Intrinsic Atomic Orbitals: An Unbiased Bridge between Quantum Theory and Chemical Concepts. *J. Chem. Theory Comput.* **2013**, *9*, 4834–4843.
- (36) Jess, K.; Baabe, D.; Bannenberg, T.; Brandhorst, K.; Freytag, M.; Jones, P. G.; Tamm, M. Ni-Fe and Pd-Fe Interactions in Nickel(II) and Palladium(II) Complexes of a Ferrocene-Bridged Bis(imidazolin-2-imine) Ligand. *Inorg. Chem.* **2015**, *54*, 12032–12045.
- (37) Mahabiersing, T.; Luyten, H.; Nieuwendam, R. C.; Hartl, F. Synthesis, Spectroscopy and Spectroelectrochemistry of Chlorocarbonyl {1,2-Bis[(2,6-diisopropylphenyl)imino]acenaphthene-κ<sup>2</sup>-N,N'}-rhodium(I). *Collect. Czech. Chem. Commun.* **2003**, *68*, 1687–1709.
- (38) Dolomanov, O. V.; Bourhis, L. J.; Gildea, R. J.; Howard, J. A. K.; Puschmann, H. OLEX2: a complete structure solution, refinement and analysis program. *J. Appl. Crystallogr.* **2009**, *42*, 339–341.
- (39) Perdew, J. P.; Burke, K.; Ernzerhof, M. Generalized Gradient Approximation Made Simple [Phys. Rev. Lett. *77*, 3865 (1996)]. *Phys. Rev. Lett.* **1997**, *78*, 1396–1396.
- (40) Grimme, S.; Antony, J.; Ehrlich, S.; Krieg, H. A consistent and accurate ab initio parametrization of density functional dispersion correction (DFT-D) for the 94 elements H-Pu. *J. Chem. Phys.* **2010**, *132*, 154104.
- (41) Weigend, F.; Ahlrichs, R. Balanced basis sets of split valence, triple zeta valence and quadruple zeta valence quality for H to Rn: Design and assessment of accuracy. *Phys. Chem. Chem. Phys.* **2005**, *7*, 3297–3305.
- (42) Weigend, F.; Häser, M.; Patzelt, H.; Ahlrichs, R. RI-MP2: optimized auxiliary basis sets and demonstration of efficiency. *Chem. Phys. Lett.* **1998**, *294*, 143–152.
- (43) Neese, F. The ORCA program system. *WIREs Comput. Mol. Sci.* **2012**, *2*, 73–78.
- (44) Takano, Y.; Houk, K. N. Benchmarking the Conductor-like Polarizable Continuum Model (CPCM) for Aqueous Solvation Free Energies of Neutral and Ionic Organic Molecules. *J. Chem. Theory Comput.* **2005**, *1*, 70–77.
- (45) Brookhart, M.; Grant, B.; Volpe, A. F. [(3,5-(CF<sub>3</sub>)<sub>2</sub>C<sub>6</sub>H<sub>3</sub>)<sub>4</sub>B]<sup>-</sup>[H(OEt<sub>2</sub>)<sub>2</sub>]<sup>+</sup>: a convenient reagent for generation and stabilization of cationic, highly electrophilic organometallic complexes. *Organometallics* **1992**, *11*, 3920–3922.
- (46) Hayashi, T.; Konishi, M.; Yokota, K.-i.; Kumada, M. Cross-Coupling of Tertiary Alkyl Grignard Reagents with β-Bromostyrene Catalyzed by Dichloro[1,1'-Bis(diphenylphosphino)ferrocene]nickel(II). *Chem. Lett.* **1980**, *9*, 767–768.